H-bond weakening through π systems: Resonance-Impaired Hydrogen Bonds (RIHB)

José Manuel Guevara-Vela[a], Eduardo Romero-Montalvo[b], Alejandra del Río-Lima[b], Ángel Martín Pendás[a], Marcos Hernández-Rodríguez[b], Tomás Rocha Rinza[b,*]

[a] *Departament of Analytical and Physical Chemistry, University of Oviedo, E-33006, Oviedo, Spain.*
[b] *Institute of Chemistry, National Autonomous University of Mexico, Circuito Exterior, Ciudad Universitaria, Delegación Coyoacán C.P. 04510, Mexico City, Mexico.*

Abstract

We introduce in this contribution the concept of Resonance Impaired Hydrogen Bonds (RIHB), to describe interactions in which a network of conjugated bonds strongly hinders an H-bond (HB). For this purpose, we examine the intramolecular RIHB between the extremes of the conjugated base of 3-amino acrylaldehyde, i.e., H–N=CH–CH=CH–O^- which has a formation energy considerably lower (at least 8 kcal/mol) as compared with typical σ HBs involving charged species. The Interacting Quantum Atoms (IQA) energy partition indicates that despite the non-zero net charge of the fragments involved in these RIHB, these interactions present smaller total IQA classical interactions (comprising the sum of electrostatic attractions, charge transfer and charge and polarisation) than other neutral Resonance Assisted Hydrogen Bonds (RAHB) and σ HBs. As opposed to typical RAHBs, the occurrence of an RIHB involves an increase in the covalent bond order of double bonds, whereas single bonds exhibit the opposite behaviour as revealed by electron delocalisation. We found nevertheless that the lack of aromaticity is not a source of destabilisation for RIHBs. Altogether, we expect that this research will contribute to the understanding of the intricate interplay between hydrogen bonds and conjugated π systems.

Keywords:

Resonance-Assisted Hydrogen Bond, Resonance-Impaired Hydrogen Bond, Interacting quantum atoms, Quantum Theory of Atoms in Molecules, Electronic Localisation Function.

*To whom correspondence should be addressed: tomasrocharinza@gmail.com

Introduction

Hydrogen Bond (HB) cooperative/anticooperative effects, i.e. the mutual strengthening/weakening of two or more HBs, are crucial in the structure and stability of molecules and supramolecular clusters that present these interactions.[1, 2] For example, the oxygen-oxygen distance in small water clusters is reduced due to HB cooperativity [3], and the relative energy of the isomers of the H_2O hexamer is determined by a balance between the number of H-bonds in the system and their non-additive properties [4]. The H-bond cooperative effects in O–H···O–H motifs were recently used to explain the bifunctional catalytic role of $(H_2O)_2$ and $(H_2O)_3$ in the formation of H_2SO_4 in acid rain and the hydrolysis of CO_2 in the generation of H_2CO_3. [5] Such H-bond non-additivity has been related to the flow of charge density from the H-bond acceptor to the H-bond donor occurring throughout σ bonds, as for instance in hydrogen cyanide chains [6]

$$\text{H–C}{\equiv}\text{N}\cdots\text{H–C}{\equiv}\text{N}\cdots\text{H–C}{\equiv}\text{N}\cdots\text{H–C}{\equiv}\text{N},$$

which display a significantly enhanced HCN dipole moment as compared with its *in vacuo* value, contributing to the large dielectric constant of this compound in the liquid phase. [7] Other examples of redistribution of charge density that lead to H-bond non-additivity are those occurring in double H-bond donors and acceptors which lead to HB anticooperativity in antidromic cycles [4].

Charge transfers leading to H-bond cooperative and anticooperative effects can also occur across networks of π bonds. For instance, Wu and coworkers [8, 9] associated H-bond strengthening and weakening with the occurrence of aromaticity and antiaromaticity in dimers of π-conjugated heterocycles as well as acyclic amides and amidines. Resonance-Assisted Hydrogen Bonds (RAHB)[10–12] constitute other relevant systems in which the interplay between a conjugated π network and an H-bond strengthen the latter interaction. The simple classical resonance structures of malondialdehyde **1** and 3-amino acrylaldehyde **2** shown in Figure 1 suggest

- a strengthening of the H···O bond in the HB acceptor and

- a weakening of the X–H linkage (X = O, N in **1** and **2** respectively).

Both conditions contribute to making the intramolecular H-bond in **1** and **2** stronger as compared with σ OH···O and NH···O HBs. Two hydrogen bonds can also be connected throughout RAHBs to exert cooperative and anticooperative effects on each other [13, 14].

On the other hand, Figure 1 shows the intramolecular H-bond in the conjugated base of **2** [†], namely, anion **3**. The resonance structure shown in this figure suggests that the electron-drawing nature of the HN=CH–CH group makes the hydrogen bond donor (i.e., the imine group) richer in electrons. Concomitantly, the corresponding acceptor loses electron density through the network of conjugated bonds. These two facts weaken the intramolecular HB in **3**. In other words, the π system in this anion hinders the intramolecular HB, that is to say, we are in front of a *Resonance Impaired Hydrogen Bond* (RIHB) as introduced in this paper.

More specifically, this investigation focuses on a comparison of RAHB and RIHB, and it is aimed to provide insights into the factors which cause that a π system strengthens or weakens a given H-bond. For that purpose, we have compared the RAHBs in **2** and the RIHB in **3** with the similar intermolecular H-bonds

$$\mathrm{CH_2{=}CH{-}NH{-}H{\cdots}O{=}CH{-}CH{=}CH_2} \qquad \mathbf{2}_{\mathrm{inter}}$$

$$\mathrm{H_2C{=}CH{-}CH{=}N{-}H{\cdots}{}^{-}O{-}CH{=}CH_2} \qquad \mathbf{3}_{\mathrm{inter}}$$

which are denoted as $\mathbf{2}_{\mathrm{inter}}$ and $\mathbf{3}_{\mathrm{inter}}$ respectively as illustrated in Figure 2. Both the HB donors and acceptors in $\mathbf{2}_{\mathrm{inter}}$ and $\mathbf{3}_{\mathrm{inter}}$ are conjugated to make a better comparison with the intramolecular H-bonds in **2** and **3**. We have used quantum chemical topology tools, namely the Quantum Theory of Atoms in Molecules (QTAIM), the Interacting Quantum Atoms (IQA) partition of the electronic energy and the analysis of the Electronic Localisation Function (ELF) to get further insights about the factors stabilising resonance assisted and impaired hydrogen bonds. These methods of wavefunction analyses are based on the first-order reduced

[†]This species is generated by the loss of an N-H hydrogen and the subsequent tautomerization to the enolate, in virtue that an enol is more acidic than an enamine.

density matrix $\varrho_1(\mathbf{r}_1, \mathbf{r}_1')$ and on the one- and two- electron density functions $\varrho_1(\mathbf{r}_1)$ and $\varrho_2(\mathbf{r}_1, \mathbf{r}_2)$. We use these approaches because they have provided valuable information about the nature of H-bond cooperativity and anticooperativity occurring both across σ and π bonds [4, 5, 13, 15, 16]. All in all, our results establish relevant differences between RAHBs and RIHBs and hence we expect they will help in the understanding of the complicated interplay between H-bonds and π conjugated systems.

Methods

The methodologies used for the analysis of resonance assisted and resonance impaired hydrogen bonds should be suitable to describe interactions in the long and short-distance regimes. This circumstance arises because part of the account presented herein concerns the mutual effect between the conjugated π system and the H bonds occurring in RAHBs and RIHBs. Hence, we have decided to use methods that can account for both HBs and electron delocalisation on the same footing, i.e., through the study of scalar fields derived from the electronic state vector such as the charge distribution $\varrho(\mathbf{r})$ and the pair density $\varrho_2(\mathbf{r}_1, \mathbf{r}_2)$.

The investigation of these scalar fields is best done through real space theories of chemical bonding such as the QTAIM. This approach is built upon the topology of $\varrho(\mathbf{r})$ which allows a partition of three dimensional space into disjoint regions associated with atoms forming functional groups, molecules and molecular clusters. In this way, the QTAIM provides a seamless link between short and long range interactions. QTAIM basins can be understood as proper open quantum mechanical subsystems for which one can obtain well-behaved expectation values of Dirac observables.

We can also use the QTAIM to analyse the changes in the chemical bonding scenario when a given intramolecular H-bond is formed or dissociated. For this purpose, we have considered the integration of the exchange-correlation hole over the topological atoms to calculate so-called Delocalization Indices (DI) [17]

$$\delta(\Omega, \Omega') = 2 \left| \int_{\Omega} \int_{\Omega'} \varrho(\mathbf{r}_1) \varrho(\mathbf{r}_2) f(\mathbf{r}_1, \mathbf{r}_2) \mathrm{d}\mathbf{r}_1 \mathrm{d}\mathbf{r}_2 \right|, \tag{1}$$

wherein $\Omega \neq \Omega'$ i.e., Ω and Ω' are two different atoms, and $f(\mathbf{r}_1, \mathbf{r}_2)$ is the correlation factor relating the pair density $\varrho_2(\mathbf{r}_1, \mathbf{r}_2)$ and $\varrho(\mathbf{r})$ [18]

$$\varrho_2(\mathbf{r}_1, \mathbf{r}_2) = \varrho(\mathbf{r}_1)\varrho(\mathbf{r}_2)(1 + f(\mathbf{r}_1, \mathbf{r}_2)). \tag{2}$$

The DI $\delta(\Omega, \Omega')$ is a measure of the number of electrons shared between two atoms Ω and Ω' and therefore of the covalency of the bond between them.

Finally, electron delocalization is intimately related to other chemical phenomena such as aromaticity. We used DIs to compute the aromaticity indices (i) $\mathrm{I_{ring}}(\mathscr{A})$, a measurement involving the sum of the σ and π electron populations [19], (ii) $\mathrm{MCI}(\mathscr{A})$, which assess the values of delocalisation in comparison with those of benzene [20], and finally (iii) $\mathrm{I_{NG}}(\mathscr{A})$ together with (iv) $\mathrm{I_{NB}}(\mathscr{A})$, that utilize the Hückel molecular orbital approximation to match the topological resonance energies per π electron of aromatic annulenes and their ions [21]. within the pseudocycles of systems **2** and **3**. We proceeded in this way in virtue of the relation that can exist between aromaticity, antiaromaticity and H-bond strength briefly discussed in the introduction.

Despite the definition of DIs in QTAIM, the theoretical framework of this approach yields only one-atom contributions to the total electronic energy. One is often interested in how the interaction energy between two atoms or functional groups is affected when it occurs a change in the system of interest. The IQA energy partition offers a solution to this situation, by considering the one- and two-domain division of the non-relativistic Born-Oppenheimer electronic energy, [22]

$$E = \sum_{\mathrm{X}} E^{\mathrm{X}}_{\mathrm{net}} + \sum_{\mathrm{X>Y}} E^{\mathrm{XY}}_{\mathrm{int}} = \sum_{\mathrm{X}} T^{\mathrm{X}} + V^{\mathrm{XX}}_{\mathrm{ne}} + V^{\mathrm{XX}}_{\mathrm{ee}} + \sum_{\mathrm{X>Y}} V^{\mathrm{XY}}_{\mathrm{nn}} + V^{\mathrm{XY}}_{\mathrm{ne}} + V^{\mathrm{YX}}_{\mathrm{ne}} + V^{\mathrm{XY}}_{\mathrm{ee}}, \tag{3}$$

wherein $E^{\mathrm{X}}_{\mathrm{net}}$ and $E^{\mathrm{YZ}}_{\mathrm{int}}$ are the IQA net and interaction energies of atom X and pair YZ. The quantity T^{X} represents the contribution to the kinetic energy from basin X. Finally, the terms $V^{\mathrm{XY}}_{\mathrm{ne}}$ and $V^{\mathrm{XY}}_{\mathrm{ee}}$ denote (i) the attraction between the nucleus of domain X and the electrons of basin Y and (ii) the repulsion of electrons in X and Y. The conditions X = Y and X ≠ Y correspond respectively to intra- and inter-atomic contributions to the electronic energy.

It is possible to get further insight into the nature of the interaction between two atoms by considering the Coulombic and exchange-correlation components of the electronic repulsion, which allows to split the IQA interaction energy between two atoms into classical (or coulombic) ($V_{\mathrm{cl}}^{\mathrm{XY}}$) and exchange-correlation ($V_{\mathrm{xc}}^{\mathrm{XY}}$) contributions [22]

$$E_{\mathrm{int}}^{\mathrm{XY}} = V_{\mathrm{cl}}^{\mathrm{XY}} + V_{\mathrm{xc}}^{XY}. \tag{4}$$

The intra-atomic potential energy can also be partitioned as indicated in equation (4) in $V_{\mathrm{cl}}^{\mathrm{X}}$ and $V_{\mathrm{xc}}^{\mathrm{X}}$.

As the QTAIM provides an atomic partition of an electronic system, other scalar fields related to the localisability of electrons have shown their ability to partition the 3D space into the traditional core, lone and bonding pairs of chemistry. One of the best known is the Electron Localisation Function (ELF) introduced by Becke and Edgecombe [23], which has been extensively used after the work of Savin and Silvi [24]. The ELF, initially defined for Hartree-Fock wave functions only, was further generalised by Savin [25], who related it to the excess kinetic energy density of an electron system with respect to the bosonic von Weizsäcker reference. The evolution of ELF basins along a chemical process has been shown to correlate well with standard chemical wisdom, particularly when lone pairs play a significant role as it is the case in this contribution.

Computational details

Previous studies [26] have indicated that hydrogen bonding is well described in second order Møller-Plesset perturbation theory employing augmented Dunning basis sets. For this reason, all geometries in the present work were obtained using the MP2 [27] method in its efficient RIJCOSX variant [28] in conjunction with the aug-cc-pVTZ basis set [29] as implemented in the Orca software [30]. Harmonic frequencies calculations were performed to confirm that the optimised structures correspond indeed to local minima.

The QTAIM and IQA analyses were made with our Promolden code [31] using B3LYP/ aug-cc-pVTZ electron densities, which were read directly from the Orca output files with the aid of the program Molden2Aim [32, 33]. This methodology has succesfully been used along

with quantum chemical topology in the study of RAHBs. [34] We considered an approximation to the one- and two-atom terms of the Kohn-Sham exchange-correlation energy [35] to perform the IQA energy partition. β-spheres of between 0.1 and 0.3 bohr of radii were used through the computation along with restricted angular Lebedev quadratures. This range of radii was selected as a compromise between the needed accuracy and the associated computational cost. There are two choices regarding the size of β-spheres in IQA integrations that usually give good results. (i) Small β-spheres are useful to eliminate the nuclear singularities, while (ii) large β-spheres (with radii typically equal to 90% the distance to the closest bond critical point) take advantage of the shape of the volume to integrate using a coarser grid in as much space as possible, thus reducing the computational effort. We observed that the former approach resulted in better IQA total energies for the systems studied herein, and hence it was the procedure chosen in this investigation. Inside the β-spheres, 451 mapped radial point trapezoidal quadratures and L expansions truncated at l =10 were employed; while outside the β-spheres the number of mapped radial points was increased to 651 and L up to l =12 was used.

The ELF analysis were also carried out using the in-house code PROMOLDEN, available upon request [31]. The aromaticity indices, $I_{\text{ring}}(\mathscr{A})$, $I_{\text{NG}}(\mathscr{A})$ $I_{\text{NB}}(\mathscr{A})$ and MCI($\mathscr{A}$) were computed with the software ESI-3D [36]. Finally, the software AVOGADRO [37] was used to visualise molecular structures.

Results and discussion

Electronic structure calculations

Table 1 shows the electronic structure results on the formation energy of the hydrogen bonds in **2** and **3** along with the respective intermolecular H-bonds with which they are compared, i.e., $\mathbf{2}_{\text{inter}}$ and $\mathbf{3}_{\text{inter}}$. As expected, the interaction between the H-bonded atoms and the π system in the RAHB increases the formation energy of the HB. We estimate the energetic effect of the RAHB as

$$\Delta\Delta E_{\text{RAHB}} = \Delta E_{\text{form}}^{\text{H bond}}(\mathbf{2}) - \Delta E_{\text{form}}^{\text{H bond}}(\mathbf{2}_{\text{inter}}) = -4.3 \text{ kcal/mol}. \quad (5)$$

On the contrary, the interaction between the hydrogen bond donor and acceptor in anion **3** reduces quite noticeably the formation of the HB in comparison with the H-bond in $\mathbf{3}_{\text{inter}}$. Likewise to equation (5), the RIHB effect reduces the magnitude of $\Delta E_{\text{form}}^{\text{H bond}}$ by

$$\Delta\Delta E_{\text{RIHB}} = \Delta E_{\text{form}}^{\text{H bond}}(\mathbf{3}) - \Delta E_{\text{form}}^{\text{H bond}}(\mathbf{3}_{\text{inter}}) = 11.7 \text{ kcal/mol}. \quad (6)$$

Indeed, the absolute value of the formation energy of the intramolecular H-bond in anion **3**, $|\Delta E_{\text{form}}^{\text{RIHB}}(\mathbf{3})| = 2.6$ kcal/mol (Figure 1), is significantly lower than the corresponding energies for typical σ HBs which include charged species. The magnitudes of $\Delta E_{\text{form}}^{\text{H bond}}$ for these systems are usually larger than 10 kcal/mol, like that of $\mathbf{3}_{\text{inter}}$ ($|\Delta E_{\text{form}}^{\text{H bond}}(\mathbf{3}_{\text{inter}})| =$ 14.3 kcal/mol), and can be as large as 30 – 40 kcal/mol in the strongly bonded, symmetric $[H_2O{\cdots}H{\cdots}OH_2]^+$ and $[F{\cdots}H{\cdots}F]^-$ molecules. [2]

Not only the energetics but also the H···O and H···O distances resulting from the formerly described electronic structure calculations indicate the respective stabilizing/destabilizing effect of the π system on the RAHB and RIHB examined herein. [†] Table 2 reports these parameters for the HBs in **2**, $\mathbf{2}_{\text{inter}}$, **3** and $\mathbf{3}_{\text{inter}}$ which indicate how the surrounding conjugated bonds strengthen/weaken the examined RAHB/RIHB.

To get further insight about the reasons underlying the opposite effects found in the intramolecular H-bonds examined herein, we now turn to dissect our results in the light of the wavefunction analyses performed through the QTAIM, IQA and ELF approaches already summarised.

Quantum chemical topology

RAHBs have been previously characterised through quantum chemical topology as interactions which involve a homogenisation of the DIs through the pseudocycle forming the H-bond structure as shown in Figure 3 (a) [5, 16]. In other words, the number of shared electron

[†]The angle $\theta = \measuredangle$(X–H···Y) is also a parameter which indicates the strenghth of the H-bond X–H···Y. A stronger HB is usually related with a larger value of θ. [2] Nonetheless, the geometric contraints imposed by the pseudocycles in **2** and **3** prevent to use θ to compare the examined RAHB and RIHB with those in $\mathbf{2}_{\text{inter}}$ and $\mathbf{3}_{\text{inter}}$ respectively.

associated with the double bonds decrease while the number of those related to the single bonds show the opposite behaviour, in agreement with the arrow pushing sketched in Figures 1 (a) and (b) and Figure 4 (a). On the contrary, the formation of the RIHB makes the delocalisation indices through the pseudocycle less uniform (Figure 3 (b)), i.e., double/single bonds increase/decrease their DIs after the occurrence of this interation as shown in Figure 4 (b). Thus, the π conjugated channels in RAHB and RIHB behave in opposite ways concerning the effects of bond order in double and single bonds after the formation of the corresponding HBs. The intermolecular H-bonds used as control systems, $\mathbf{2}_{\text{inter}}$ and $\mathbf{3}_{\text{inter}}$ have a similar behaviour to **2** and **3** respectively concerning the change in the DIs for single and double bonds, as displayed in Figure S1. We also note that the diminution of the DI associated to the N–H bond because of the formation of the HB is larger for the RAHB as compared with the RIHB, in consistency with the fact that the former interaction is a stronger hydrogen bond.

The changes in the DIs in Figure 3 suggest that system **3** will have a larger aromatic character than system **2**. Indeed, as shown in Table 3, the well established multi-center aromaticity indices $\text{I}_{\text{ring}}(\mathscr{A})$ [19], that measures the 6-center delocalization along the direct ring path, $\text{MCI}(\mathscr{A})$ [20], which adds all the other possible paths, as well as their normalized versions, $\text{I}_{\text{NG}}(\mathscr{A})$ and $\text{I}_{\text{NB}}(\mathscr{A})$ [21] indicate, to different degrees, that compound **3** is more aromatic than compound **2**. Hence, although normally it is considered that aromaticity is a source of stabilization, what we found here is that the most stable compound is the least aromatic. This surprising result is in close agreement with our previous work indicating that the strength of RAHB compared with those in non-conjugated carbonyl molecules is not originated in its resonant structures [16].

The variations in the delocalisation indices indicated in Figure 3 due to the formation of the RAHB and RIHB is supported by the analysis of the ELF in Figure 5, which shows several isosurfaces of this scalar field. The electron population associated with a given domain increases with the size of the isosurface. The C_1–C_2 and C_2–C_3 bonds (the atom numbering is shown in Figure 3) in system **2** are qualitatively more similar upon the formation of the HB whereas the opposite occurs in the case of anion **3**. Additionally, the examination of the ELF in molecule **2** in its open conformer reveals a solitary lone pair (Figure 5 (a)), which

disappears when the RAHB is formed. This last result indicates a substantial conjugation of this lone pair with the adjacent C–N bond upon the formation of the resonance-assisted HB. The base **3** does not exhibits such lone pair either in the dissociated or in the H-bonded conformation.

As discussed before, [16] the fact that the RAHB makes the bond orders more uniform through the π system does not imply that the number of delocalised electrons increases with the formation of this H-bond. Similarly, the reduced uniformity in the DIs following the formation of the RIHB in **3** is not accompanied by a decrease in the total number of delocalised electrons. These statements are based on the sum rule obeyed by the localisation and delocalisation indices

$$N = \sum_{\mathrm{X}} \lambda(\mathrm{X}) + \frac{1}{2} \sum_{\mathrm{X} \neq \mathrm{Y}} \delta(\mathrm{X}, \mathrm{Y}) \tag{7}$$

where the total number of electrons in a molecule is partitioned into localised (as measured by λ, the atomic localisation index) and delocalised sets (as measured by the interatomic DIs).

Table 4 shows that the total number of delocalised electrons is slightly reduced after the formation of the RAHB in **2** while the number of delocalised electrons almost remain constant in system **3** on account of the formation of the RIHB. The increase of the number of localised electrons in **2** as a consequence of the RAHB is accompanied by a substantial rise in in the intra-atomic component of the IQA exchange-correlation energy, $\Delta|\sum_{\mathrm{A}} V_{\mathrm{xc}}^{\mathrm{A}}|$ = 23.9 kcal/mol. Interestingly, the interatomic exchange becomes less negative $\sum_{\mathrm{A>B}} \Delta V_{\mathrm{xc}}^{\mathrm{AB}}$ = 17.5 kcal/mol. As previously discussed, [16] an important source of stabilisation from the RAHB comes from the change of the intra-atomic component of electron exchange rather than the inter-atomic exchange as suggested by the mesomeric structures in Figure 1 (a) and (b). We have found similar effects concernig the intra $\sum_{\mathrm{A}} \Delta V_{\mathrm{xc}}^{\mathrm{A}}$ and the inter $\sum_{\mathrm{A>B}} \Delta V_{\mathrm{xc}}^{\mathrm{AB}}$ in the RIHB here examined, but considerably smaller in magnitude.

The behaviour of the delocalisation indices after the generation of an RAHB or RIHB indicates that the pair density is affected in different ways due to these interactions. Because the charge distribution can be obtained by integrating $\varrho_2(\mathbf{r}_1, \mathbf{r}_2)$ then we expect distinct modifications of $\varrho(\mathbf{r})$ in resonance-assisted and impaired hydrogen bonds. For example, Table

5 shows that RAHBs and RIHBs involve qualitatively similar changes in QTAIM charges. Nonetheless, the variations in $q(\Omega)$ are more conspicuous for the former HB than for the latter, in agreement with the above comparison of these interactions.

The smaller rearrangement of charge distribution in the RIHB as compared with the RAHB is consistent with the fact that the absolute values of all the components of the IQA decomposition of the formation energy of the former interaction are significantly lower than that of the latter H-bond (Table 6). We stress that even the IQA classical contribution, which jointly takes into account the electrostatics, polarisation and charge transfer energies in standard energy decomposition analyses is smaller in the examined RIHBs than in the RAHBs, although the resonance-impaired H-bond involves a negatively charged enolate as the HB acceptor. Additionally, Table 6 indicates that the magnitude of $\sum_{\mathrm{A>B}} \Delta V_{\mathrm{cl}}^{\mathrm{A>B}}$ for the H-bond $\mathbf{3}_{\mathrm{inter}}$ corresponding to the intermolecular interaction of an enolate and an α-β unsaturated imine is more than twice the corresponding value for the RIHB in **3**. This chart also reveals that the most important sources of stabilisation in the investigated H-bonds are $\sum_{\mathrm{A>B}} \Delta V_{\mathrm{cl}}^{\mathrm{AB}}$ and $\sum_{\mathrm{A>B}} \Delta V_{\mathrm{xc}}^{\mathrm{A}}$, the first component being more important than the second. As a matter of fact, the order of the absolute values of the change of these components after the formation of the H-bond

$$\begin{aligned} |\Delta V_{\mathrm{cl}}^{\mathrm{AB}}|(\mathbf{3}_{\mathrm{inter}}) > |\Delta V_{\mathrm{cl}}^{\mathrm{AB}}|(\mathbf{2}) > |\Delta V_{\mathrm{cl}}^{\mathrm{AB}}|(\mathbf{2}_{\mathrm{inter}}) > |\Delta V_{\mathrm{cl}}^{\mathrm{AB}}|(\mathbf{3}), \\ |\Delta V_{\mathrm{xc}}^{\mathrm{A}}|(\mathbf{3}_{\mathrm{inter}}) > |\Delta V_{\mathrm{xc}}^{\mathrm{A}}|(\mathbf{2}) > |\Delta V_{\mathrm{cl}}^{\mathrm{A}}|(\mathbf{2}_{\mathrm{inter}}) > |\Delta V_{\mathrm{cl}}^{\mathrm{A}}|(\mathbf{3}), \end{aligned} \tag{8}$$

is the same than that of the formation energies discussed in the previous subsection

$$|\Delta E_{\mathrm{form}}^{\mathrm{AB}}|(\mathbf{3}_{\mathrm{inter}}) > |\Delta E_{\mathrm{form}}^{\mathrm{AB}}|(\mathbf{2}) > |\Delta E_{\mathrm{form}}^{\mathrm{AB}}|(\mathbf{2}_{\mathrm{inter}}) > |\Delta E_{\mathrm{form}}^{\mathrm{AB}}|(\mathbf{3}). \tag{9}$$

Similar tendencies are observed for the interaction O···H as reported in Table 7. The magnitude of the exchange-correlation component for the N−H bond decreases in the inverse order as in inequalities (8) and (9),

$$|V_{\mathrm{xc}}^{\mathrm{N-H}}|(\mathbf{3}) > |V_{\mathrm{xc}}^{\mathrm{N-H}}|(\mathbf{2}_{\mathrm{inter}}) > |V_{\mathrm{xc}}^{\mathrm{N-H}}|(\mathbf{2}) > |V_{\mathrm{xc}}^{\mathrm{N-H}}|(\mathbf{3}_{\mathrm{inter}}) \tag{10}$$

in agreement with the relative strenghts of the H-bond considered herein, as a more covalent

N–H bond indicates a weaker H···O HB.

Concluding remarks

We have introduced in this paper the concept of Resonance Impaired Hydrogen Bond, i.e., an HB substantially hindered by a surrounding π system. The consideration of intermolecular hydrogen bonds as control systems shows that the examined RIHB has a low formation energy despite a negative charge in the enolate group acting as the H-bond acceptor. While typical charged σ H-bonds have formation energies that usually surpass 10 kcal/mol, the corresponding value for the examined RIHB in this work is $\Delta E_{\text{form}}^{\text{RIHB}}$ = −2.6 kcal/mol. The QTAIM and ELF analyses indicate that RAHBs and RIHB behave differently concerning the homogenization of bond orders throughout the pseudocycle formed in these interactions. Different aromaticity indices indicate that anion **3** is more aromatic than molecule **2** despite the RAHB is stronger than the RIHB. This result being consistent with previous descriptions of RAHB in which the stability of this HB is not based in the corresponding mesomeric structures. Instead, both RAHBs and RIHBs become stabilised through intra-atomic exchange as well as electrostatic effects as shown by the IQA energy partition. Nonetheless, the magnitude of these effects is larger in an RAHB than it is in an RIHB. We expect overall that these results give valuable insights in the complex interplay between π conjugated systems and H-bonds in chemistry.

Acknowledgements

The authors acknowledge financial support from the Spanish goverment (grant CTQ-2015-65790-P) as well as computer time from DGTIC/UNAM (grant LANCAD-UNAM-DGTIC-250) T.R-R., E.R.M. and J.M.G.V. are also grateful to CONACyT/México for financial support (grant 253776), a M.Sc. and PhD. scholarships (numbers 308773 and 381483) respectively. T. R.-R. is also thankful to Magdalena Aguilar Araiza, Gladys Cortés Romero and David Vazquez Cuevas for technical support.

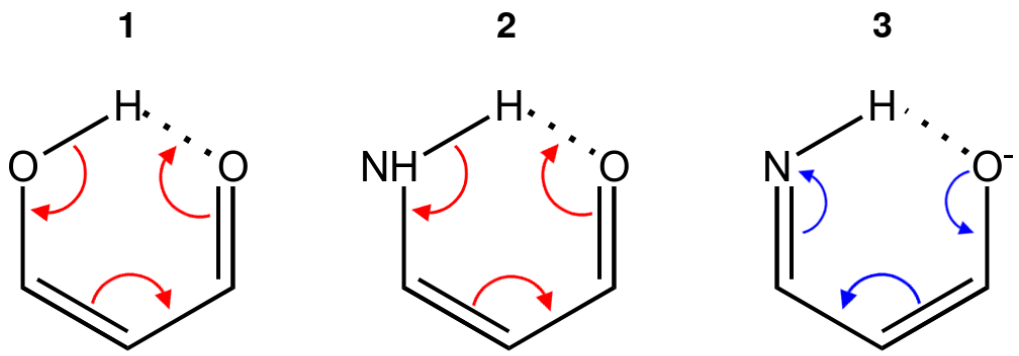

Figure 1: Resonance-assisted hydrogen bonds in malondialdehyde, **1**, and 3-amino acrylaldehyde, **2**. The resonance-impaired hydrogen bonds in the conjugated base of **2**, i.e. compound **3** is shown as well. The arrow pushing shown in red/blue strengthens/weakens the schematised H bonds.

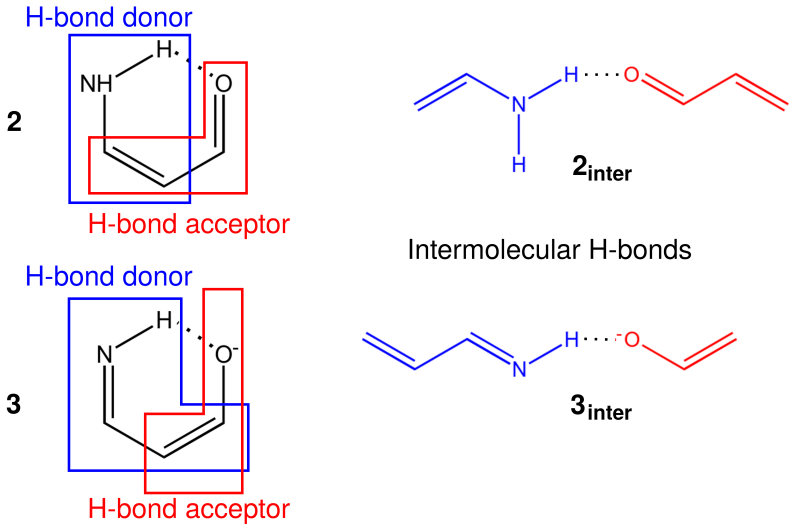

Figure 2: Intermolecular hydrogen bonds $\mathbf{2_{inter}}$ and $\mathbf{3_{inter}}$ used to examine (i) the resonance assisted hydrogen bond in 3-amino acrylaldehyde **2** and (ii) the resonance impaired hydrogen bonds in its conjugated base **3** respectively. The hydrogen bond donors are indicated in blue colour while the H-bond acceptors are displayed in red.

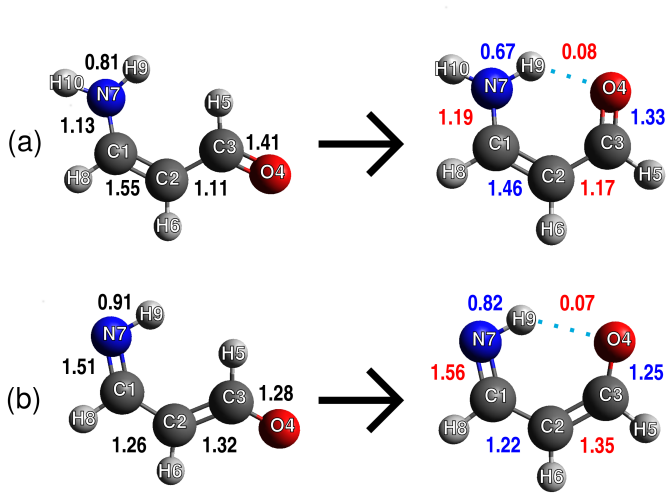

Figure 3: Changes in the delocalisation indices across the pseudocycles of (a) **2** and (b) **3** on account of the formation of the resonance assisted and impaired hydrogen bonds, respectively. An increase/decrease in $\delta(\mathrm{X},\mathrm{Y})$ as a result of the formation of these intramolecular H-bonds is indicated with red/blue.

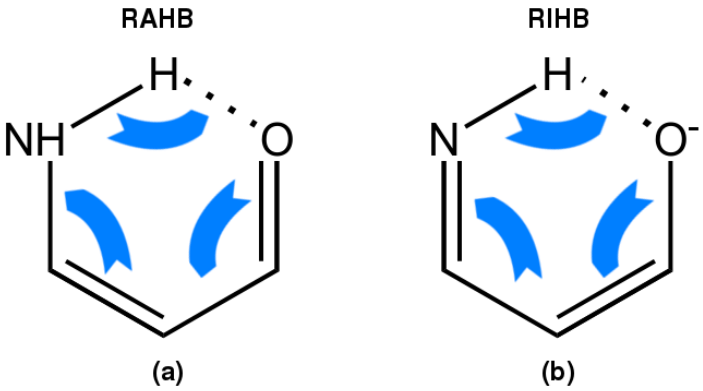

Figure 4: Flow of electron density in the pseudocycles of (a) RAHB and (b) RIHB investigated.

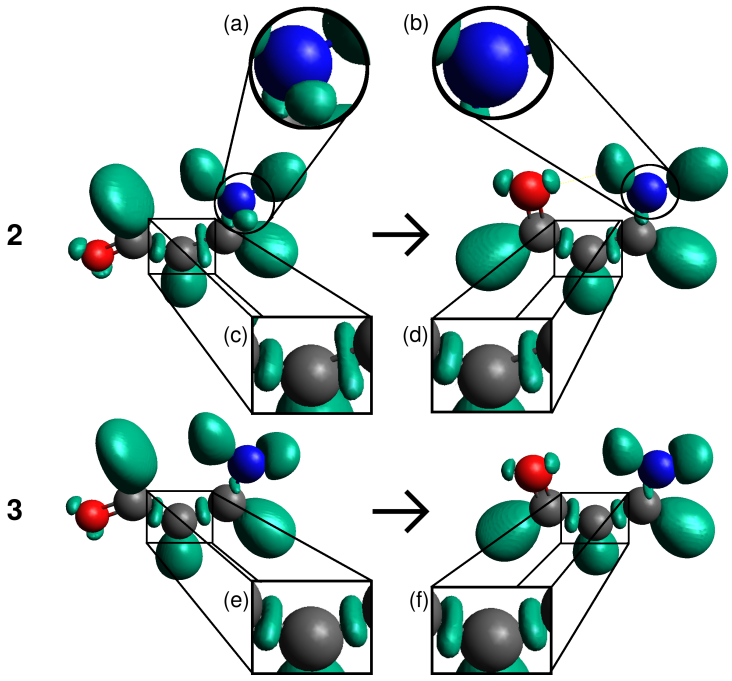

Figure 5: ELF isosurfaces at isovalue 0.9 for the RAHB **2** in its open (a) and closed (b) conformations and the RIHB **3** in its open (c) and closed (d) dispositions.

Table 1: Formation energy for the H-bonds in systems **2**, $\mathbf{2}_{\text{inter}}$, **3** and $\mathbf{3}_{\text{inter}}$. The values are reported in kcal/mol.

System	$\Delta E_{\text{form}}^{\text{H bond}}$
2	−7.9
$\mathbf{2}_{\text{inter}}$	−3.6
3	−2.6
$\mathbf{3}_{\text{inter}}$	−14.3

Table 2: O···H and N···O distances (in ångstroms) for the H-bonds in systems **2**, $\mathbf{2}_{\text{inter}}$, **3**, $\mathbf{3}_{\text{inter}}$.

System	d(H···O)	d(N···O)
2	1.896	2.665
$\mathbf{2}_{\text{inter}}$	2.024	3.030
3	2.135	2.979
$\mathbf{3}_{\text{inter}}$	1.714	2.752

Table 3: Aromaticity indices $\text{I}_{\text{ring}}(\mathscr{A})$, MCI($\mathscr{A}$), $\text{I}_{\text{NG}}(\mathscr{A})$ and $\text{I}_{\text{NB}}(\mathscr{A})$ for the closed conformations of **2** and **3**.

Index	**2**	**3**
I_{ring}	0.001211	0.001668
MCI	0.022377	0.023604
I_{NG}	0.001618	0.002265
I_{NB}	0.021824	0.023082

Table 4: Change in the number of delocalised electrons and the intra- and intermolecular components of the IQA exchange-correlation energy (reported in kcal/mol) as a consequence of the formation of the H-bonds in **2**, $\mathbf{2}_{\text{inter}}$ **3**, and $\mathbf{3}_{\text{inter}}$.

System	$\sum_{\text{A>B}} \Delta\delta(\text{A},\text{B})$	$\sum_{\text{A}} \Delta V_{\text{xc}}^{\text{A}}$	$\sum_{\text{A>B}} \Delta V_{\text{xc}}^{\text{AB}}$
2	−0.08	−23.9	17.5
$\mathbf{2}_{\text{inter}}$	−0.03	−14.9	6.2
3	0.01	−0.7	4.0
$\mathbf{3}_{\text{inter}}$	−0.01	−24.7	14.6

Table 5: Variations in the QTAIM charges in **2** and **3** on account of the formation of the respective RAHB and RIHB in these systems. The atomic numbering is shown in Figure 3. Atomic units are used throughout.

Atom	**2**	**3**	Atom	**2**	**3**
C1	0.11	0.04	H6	−0.04	−0.03
C2	−0.04	−0.03	N7	−0.10	−0.03
C3	−0.08	−0.02	H8	0.00	−0.01
O4	−0.04	0.00	H9 (H-bond)	0.12	0.11
H5	0.04	−0.01	H10	0.01	—
$\sum_{\mathrm{A}} \lvert\Delta Q(\mathrm{A})\rvert$	0.58	0.28	—	—	—

Table 6: Interacting quantum atoms partition of the formation energy of the H-bonds in **2**, $\mathbf{2}_{\mathrm{inter}}$, **3** and $\mathbf{3}_{\mathrm{inter}}$. Values in kcal/mol.

System	$\sum_{\mathrm{A>B}} \Delta\delta(\mathrm{A},\mathrm{B})$	$\sum_{\mathrm{A}} \Delta T^{\mathrm{A}}$	$\sum_{\mathrm{A}} \Delta V_{\mathrm{cl}}^{\mathrm{A}}$	$\sum_{\mathrm{A}} \Delta V_{\mathrm{xc}}^{\mathrm{A}}$	$\sum_{\mathrm{A>B}} \Delta V_{\mathrm{cl}}^{\mathrm{AB}}$	$\sum_{\mathrm{A>B}} \Delta V_{\mathrm{xc}}^{\mathrm{AB}}$
2	−0.01	16.88	43.35	−14.26	−58.36	5.52
$\mathbf{2}_{\mathrm{inter}}$	0.01	20.39	22.97	−8.46	−38.09	0.51
3	0.03	−3.49	22.42	0.93	−21.56	0.68
$\mathbf{3}_{\mathrm{inter}}$	0.04	26.56	36.27	−16.04	−62.56	3.46

Table 7: Changes in the IQA energy components, $E_{\rm int}^{\rm AB}$, $V_{\rm cl}^{\rm AB}$ and $V_{\rm xc}^{\rm AB}$ for the O···H and N–H bonds because of the formation of the HBs in the examined systems, *i.e.*, from the open to the H-bonded conformation of **2** and **3** (as shown in Figure 3) and from the dissociated to the associated forms for $\mathbf{2}_{\rm inter}$ and $\mathbf{3}_{\rm inter}$. The data are reported in kcal/mol.

	O···H			N–H		
System	$E_{\rm int}^{\rm AB}$	$V_{\rm cl}^{\rm AB}$	$V_{\rm xc}^{\rm AB}$	$E_{\rm int}^{\rm AB}$	$V_{\rm cl}^{\rm AB}$	$V_{\rm xc}^{\rm AB}$
2	−106.4	−93.7	−12.8	−297.2	−153.9	−143.3
$\mathbf{2}_{\rm inter}$	−74.7	−65.7	−8.9	−277.9	−118.0	−159.9
3	−71.1	−61.6	−9.6	−259.2	−90.4	−168.9
$\mathbf{3}_{\rm inter}$	−126.9	−104.6	−22.3	−273.7	−138.9	−134.8

References

[1] S. Scheiner, *Hydrogen Bonding. A Theoretical Perspective*, Oxford University Press, New York, **1997**.

[2] T. Steiner, *Angew. Chem. Int. Ed* **2002**, *41*, 48.

[3] K. Liu, J. D. Cruzan, R. J. Saykally, *Science* **1996**, *271*, 929.

[4] J. M. Guevara-Vela, E. Romero-Montalvo, V. A. Mora Gómez, R. Chávez-Calvillo, M. García-Revilla, E. Francisco, A. Martín Pendás, T. Rocha-Rinza, *Phys. Chem. Chem. Phys.* **2016**, *18*, 19557.

[5] E. Romero-Montalvo, J. M. Guevara-Vela, W. E. Vallejo-Narváez, A. Costales, A. Martín Pendás, T. Rocha-Rinza, *Chem. Commun.* **2017**, *53*, 3516.

[6] K. Nauta, R. E. Miller, *Science* **1999**, *283*, 1895.

[7] L. Pauling, *The nature of the chemical bond 3rd ed.*, Cornell University Press, New York, **1960**.

[8] J. I. Wu, J. E. Jackson, P. v. R. Schleyer, *J. Am. Chem. Soc.* **2014**, *136*, 13526.

[9] T. Kakeshpour, J. I. Wu, J. E. Jackson, *J. Am. Chem. Soc.* **2016**, *138*, 3427.

[10] G. Gilli, F. Bellucci, V. Ferretti, V. Bertolasi, *J. Am. Chem. Soc.* **1989**, *111*, 1023.

[11] V. Bertolasi, P. Gilli, V. Ferretti, G. Gilli, *J. Am. Chem. Soc.* **1991**, *113*, 4917.

[12] P. Gilli, V. Bertolasi, , V. Ferretti, G. Gilli, *J. Am. Chem. Soc.* **2000**, *122*, 10405.

[13] E. Romero-Montalvo, J. M. Guevara-Vela, A. Costales, A. Martín Pendás, T. Rocha-Rinza, *Phys. Chem. Chem. Phys.* **2017**, *19*, 97.

[14] V. Bertolasi, L. Pretto, G. Gilli, P. Gilli, *Acta Cryst.* **2006**, *B62*, 850.

[15] J. M. Guevara-Vela, R. Chávez-Calvillo, M. García-Revilla, J. Hernández-Trujillo, O. Christiansen, E. Francisco, A. Martín Pendás, T. Rocha-Rinza, *Chem. Eur. J.* **2013**, *19*, 14304.

[16] J. M. Guevara-Vela, E. Romero-Montalvo, A. Costales, A. Martín Pendás, T. Rocha-Rinza, *Phys. Chem. Chem. Phys.* **2016**, *18*, 26383.

[17] X. Fradera, M. A. Austen, R. F. W. Bader, *J. Phys. Chem. A* **1999**, *103*, 304.

[18] W. Koch, M. C. Holthausen, *A Chemist's guide to Density Functional Theory*, Wiley-VCH Verlag, Weinheim, **2001**.

[19] M. Giambiagi, M. S. de Giambiagi, C. D. dos Santos Silva, A. P. de Figueiredo, *Phys. Chem. Chem. Phys.* **2000**, *2*, 3381.

[20] P. Bultinck, R. Ponec, S. Van Damme, *J. Phys. Org. Chem.* **2005**, *18*, 706.

[21] J. Cioslowski, E. Matito, M. Sol, *J. Phys. Chem. A* **2007**, *111*, 6521.

[22] M. A. Blanco, Á. Martín Pendás, E. Francisco, *J. Chem. Theory Comput.* **2005**, *1*, 1096.

[23] A. D. Becke, K. E. Edgecombe, *J. Chem. Phys.* **1990**, *92*, 5397.

[24] B. Silvi, A. Savin, *Nature* **1994**, *371*, 683.

[25] A. Savin, R. Nesper, S. Wengert, T. F. Fässler, *Angew. Chem. Int. Ed.* **1997**, *36*, 1808.

[26] C. Pérez, M. T. Muckle, D. P. Zaleski, N. A. Seifert, B. Temelso, G. C. Shields, Z. Kisiel, B. H. Pate, *Science* **2012**, *336*, 897.

[27] C. Møller, M. S. Plesset, *Phys. Rev.* **1934**, *46*, 618.

[28] S. Kossmann, F. Neese, *J. Chem. Theory Comput.* **2010**, *6*, 2325.

[29] T. H. Dunning, *J. Chem. Phys.* **1989**, *90*, 1007.

[30] F. Neese, *WIREs Comput. Mol. Sci* **2012**, *2*, 73.

[31] A. Martín Pendás, E. Francisco, PROMOLDEN. *A QTAIM/IQA code*, University of Oviedo, (unpublished).

[32] Schaftenaar, G, Molden *version 5.7, a pre- and post processing program of molecular and electronic structure*, **2016**, http://www.cmbi.ru.nl/molden/molden.html.

[33] Zou, W, Molden2Aim, **2016**, http://www.molscience.com/software/Molden2AIM.

[34] S. Wojtulewski, S. J. Grabowski, *J. Mol. Struc.-THEOCHEM* **2003**, *621*, 285–291.

[35] E. Francisco, J. L. Casals-Sainz, T. Rocha-Rinza, A. Martín Pendás, *Theor. Chem. Acc.* **2016**, *135*.

[36] E. Matito, Esi-3D*: Electron Sharing Indices Program for 3D Molecular Space Partitioning*, **2015**, Institute of Computational Chemistry and Catalysis, University of Girona, Catalonia, Spain.

[37] M. D. Hanwell, D. E. Curtis, D. C. Lonie, T. Vandermeersch, E. Zurek, G. R. Hutchison, *J. Cheminf.* **2012**, *4*, 17.